NJC

Accepted Manuscript

This is an *Accepted Manuscript*, which has been through the Royal Society of Chemistry peer review process and has been accepted for publication.

Accepted Manuscripts are published online shortly after acceptance, before technical editing, formatting and proof reading. Using this free service, authors can make their results available to the community, in citable form, before we publish the edited article. We will replace this *Accepted Manuscript* with the edited and formatted *Advance Article* as soon as it is available.

You can find more information about *Accepted Manuscripts* in the Information for Authors.

Please note that technical editing may introduce minor changes to the text and/or graphics, which may alter content. The journal's standard Terms & Conditions and the Ethical guidelines still apply. In no event shall the Royal Society of Chemistry be held responsible for any errors or omissions in this *Accepted Manuscript* or any consequences arising from the use of any information it contains.

ROYAL SOCIETY OF CHEMISTRY

www.rsc.org/njc

Cite this: DOI: 10.1039/c0xx00000x

www.rsc.org/xxxxxx

ARTICLE TYPE

Three-Dimensional Graphene Hydrogels Supported Ultrafine RuO_2 Nanoparticles for Supercapacitor Electrodes

Yuying Yang, Yarong Liang, Yadi Zhang, Ziyu Zhang, Zhiming Li, Zhongai Hu*

Received (in XXX, XXX) Xth XXXXXXXXX 20XX, Accepted Xth XXXXXXXXX 20XX

DOI: 10.1039/b000000x

In the present work, three-dimensional (3D) porous framework of RuO_2/reduced graphene oxide hydrogels (RuO_2/RGOH) were prepared by a facile one-step hydrothermal method. In this hybrid hydrogel, RuO_2 nanoparticles were homogeneously dispered on the exfoliated RGO sheets. The as-prepared RuO_2/RGOH electrode shows excellent supercapacitive performances with high specific capacitance (345 F g^{-1} for 15% RuO_2 loading), good rate capability and long electrochemical cycling life (without decaying after 2000 cycles). Furthermore, the RuO_2 in the hybrid can contribute a capacitance as high as 1365 F g^{-1}, which is comparable to its theoretical value. These excellent results originate from the factors that the 3D porous network structure provides more accessible surface area and facilitates electron and proton injecting/expelling process in electrochemical reaction. This work provides a facile method for preparing graphene-based composite materials with remarkable capacitive performances.

Introduction

As a promising candidate electrode material used in supercapacitors, ruthenium oxide (RuO_2), especially amorphous hydrous RuO_2, plays an important role in the applications of supercapacitors because of its proton-electron mixed-conductive nature and remarkably high specific capacitance. It stores charges mainly via pseudocapacitance, which arises from a potential-dependent faradaic process involving the simultaneous insertion of an electron and proton. The oxidation states of ruthenium in the RuO_2 electrode change reversibly among Ru^{4+}, Ru^{3+}, and Ru^{2+}. The mechanism can be expressed by the following redox reaction[1]:

$$RuO_x(OH)_y + \delta H^+ + \delta e^- \leftrightarrow RuO_{x-\delta}(OH)_{y+\delta} \qquad (0 \le \delta \le 2)$$

It is well known that the electrochemical reaction starts from the surface of the RuO_2 particles, and thus, the accessible surface area of RuO_2 dictates their specific capacitance. However, RuO_2 particles often tend to form agglomerates, which may significantly degrade their capacitive performance due to incomplete utilization of RuO_2 during the electrochemical redox process[2, 3]. On the other hand, the electrical conductivity of the amorphous RuO_2 is slightly lower than that of the crystalline phase due to the noncontinuous oxide framework[4], which also limits the utilization of RuO_2. In order to improve the dispersion of amorphous hydrous RuO_2 particles and the electrical conductivity of electrode materials, some hybrid electrode materials, which combine RuO_2 with high surface area nanocarbons materials such as carbon black[5, 6], carbon nanotube (CNT)[7-10], carbon nanofiber (CNF)[11-14] and graphene[15-17] have been prepared. However, most of the used carbon materials in these hybrids are still unable to provide a sufficient available active surface area for exploiting the full advantages of RuO_2 pseudocapacitance and double-layer capacitance of nanocrabons materials, and consequently, their specific capacitance are limited [10,13,15].

Graphene, a single layer of carbon atoms patterned in a hexagonal lattice, has been actively investigated in supercapacitor application due to its high specific surface area, excellent conductivity, mechanical flexibility and chemical stability[18-20]. Various graphene-based hybrid materials have been prepared [21-24]. However, in most cases, the aggregation and restacking of graphene nanosheets during processing dramatically decreases the specific surface area of graphene-based electrodes, which consequently hinders the ion diffusion from the electrolyte to the electrodes and reduces the effective capacitance[25-27]. Recently, many studies have shown that graphene oxide (GO) can form a three-dimensional (3D) architecture such as graphene hydrogels or aerogels[28-30], which would effectively prevent the restacking of graphene sheets and maintain their high specific surface area. Apart from the intrinsic properties of graphene, such hydrogel are decorated with oxygen-containing functional groups (such as carboxyl, epoxyl or hydroxyl groups) and large 3D porous network structure. The residue oxygen-containing functional groups in graphene hydrogels are believed to play dual roles here. On the one hand, these hydrophilic groups can further improve the compatibility between the electrodes and the electrolyte and thus more electroactive sites are easily infiltrated by electrolyte ions for charge-transfer reactions. On the other hand, these groups can act as anchoring sites to interact with nanoparticles, enabling growth of electroactive species on the graphene hydrogels. In addition, due to the presence of these functional groups, the water

molecules can be absorbed onto the graphene sheets through chemical adsorptions or hydrogen bonding, which can act as a soft "spacer" to prevent the graphene sheets from restacking. This unique hierarchical architecture not only improves the accessibility of surface but also facilitates electrolyte ion transportation in electrodes. Consequently, assembling graphene into a 3D structure has been recognized as one of the most effective approaches for preparation of graphene-based composite materials[31]. 3D carbon support materials have good properties for applications in energy storage and conversion[32]. X. F. Wang et al[28] prepare 3D graphene/VO_2 nanobelt composite hydrogels by a facile one-step strategy. The hybrid electrode demonstrates excellent capacitive performances. In the two-electrode configuration, the graphene/VO_2 nanobelt composite hydrogel exhibits a specific capacitance of 426 F g^{-1} at 1 A g^{-1}. S. J. Bao et al[33] prepared MnO_2-wrapped graphene aerogels using a simple in situ reduction method. As a supercapacitor electrode material, the MnO_2-wrapped graphene aerogels exhibits a high reversible capacity of 210 F g^{-1} at a current density of 0.5 A g^{-1} with an excellent cycling retention of 99% after the 800th cycle. W. Wang et al[34] prepared a novel 3D hydrous ruthenium oxide (RuO_2) anchored graphene and CNT hybrid foam (RGM) architecture for high-performance supercapacitor electrodes by a simple two-step process. This hybrid shows superior electrochemical stability and excellent capacitive performance.

Taking into account these merits of graphene hydrogels, it is believed that the combination of metal oxides with graphene hydrogels can exhibit excellent capacitive performance[28,3]. Herein, we fabricated 3D porous network RuO_2/RGOH by one-step hydrothermal self-assembled route without adding any organic solvent or surfactant. In this hybrid, 3D porous graphene hydrogel will provide the electron "superhighways" for charge storage and further promotes the charge-exchanging rate of RuO_2 involving the proton and electron double injecting/expelling process. As a result, the excellent electrochemical performance is achieved due to the kinetic and structural factors such as accessible surface sites, fast ion transport, low equivalent series resistance and high conductivity.

Result and Discussion

Formation of hydrogel

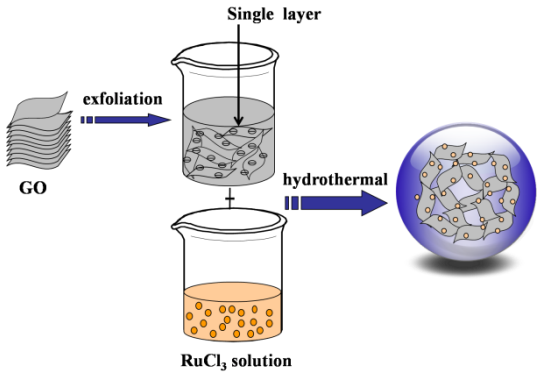

Scheme 1 Representation of the formation process of the hydrogel.

The fabrication process of the hydrogel is presented in scheme 1. Firstly, GO was exfoliated to form a stable aqueous suspension. Then certain amount of ruthenium chloride aqueous solution was slowly added into GO suspension (1.6mg mL^{-1}), see the method in the experimental section. As is well-known, GO sheets are hydrophilic and intrinsically negatively charged because of the existence of plentiful carboxyl and epoxide functionalities. Ruthenium ions are positively charged in aqueous solution. In contrast, Ru^{3+} ions will be adsorbed on GO sheets through electrostatic interactions with the C-O-C, -OH or ion-exchange with H^+ from carboxyl. Subsequently, the suspension was hydrothermally assembled to form a 3D hydrogel.

TG analyses

Thermogravimetric analysis (TG) analyses were carried out to determine the mass ratios of RuO_2 in the hybrid hydrogel. Fig. 1 shows the TG curves of hybrid hydrogel. On the TG curves, two steps of weight loss are found. The first step occurs at near 100 ℃, which is due to evaporation of physically adsorbed water from the 3D porous hydrogel. The large weight loss at about 400 ℃ is attributed to the removal of RGO from the composites. After 400 ℃, the TG traces are stable with no further weight loss, indicating the RGO completely removed from the composites. The estimations based on the TG curves indicate that mass ratios of the RuO_2 in the hybrid hydrogels are 5.2 and 15%, respectively.

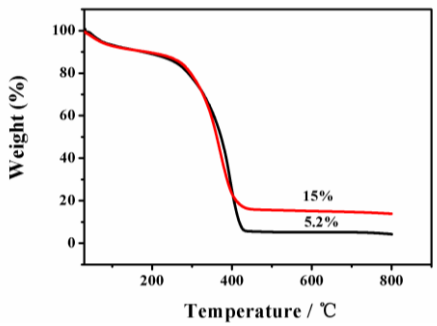

Fig. 1 TG curves of the RuO_2/RGOH.

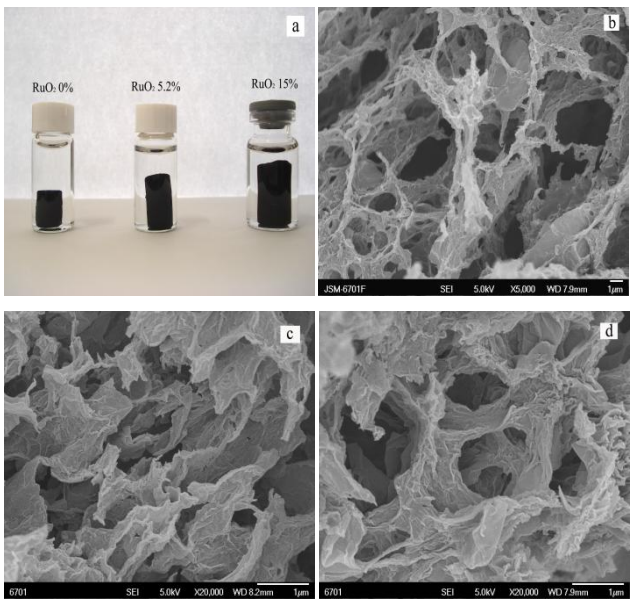

Fig. 2 (a)The photograph of RuO_2 / RGOH; FESEM images of (b) pure RGOH, (c) RuO_2-5.2%/RGOH and (d) RuO_2-15%/RGOH.

Morphology analysis

The shapes of the as-prepared hydrogels are shown Fig 2(a). As seen from the photographs, the hydrogels have a cylindrical shape. The size of the cylinders depends on the relative mass ratio of the RuO_2 in the hybrid hydrogel. The more the amount of RuO_2, the larger volume of resultant hydrogels becomes. When the mass ratio of the RuO_2 is up to 33.2%, the shape of the product was no longer integral cylinder (See Fig S1). Fig 2(b, c, d) shows the FE-SEM images of hydrogels with different mass ratios of RuO_2 to graphene in hybrid hydrogels. Plenty of pores with a wide size distribution are observed from the images, and the solid walls of these pores are composed by randomly cross-linked graphene nanosheets. The formation of 3D structured graphene hrdrogel is attributed to the partial overlapping of graphene sheets via noncovalent interactions, such as stacking and hydrogen bonding in 3D space[35, 36]. Thus, the inherent flexibility of reduced graphene oxide sheets is a crucial property for constructing the 3D macrostructures[37]. More interestingly, RuO_2 nanoparticles were not found on the surface of graphene sheets in these SEM images (Fig 2c, 2d). To further analyze the morphology of the hybrid hydrogel, the sample with 15% RuO_2 was selected for TEM observation. The TEM images in Fig 3 reveal that RuO_2/RGOH is composed of sheet-like graphene and RuO_2 particles. The RGO sheets are almost transparent with some wrinkles visible. RuO_2 nanoparticles with 2~3 nm in size are homogeneously anchored onto the surface of the RGO sheets in the hybrid hydrogel. In consider of strong sonication treatment during the preparation of TEM specimens, this observation implies the intimate interactions between RuO_2 nanoparticles and graphene sheets. The presence of oxygen-containing functional groups from graphene sheets may play an essential role in anchoring and forming fine RuO_2 nanoparticles.

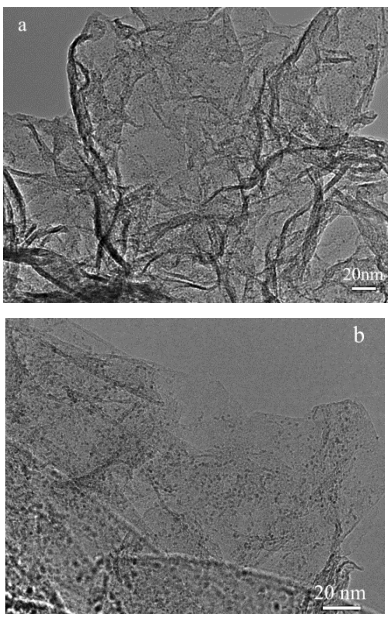

Fig. 3 TEM images of theRuO_2-15%/RGOH.

XRD analysis

The crystal phase and structure information of the products were analyzed by X-ray diffraction (XRD). Fig 4(a) shows XRD patterns of pure reduced graphene oxides hydrogel and RuO_2/RGOH. The characteristic peak located at 2θ value of about 23.4 ° is referred to the as-prepared RGO sheets. However, no discernible reflections corresponding to RuO_2 crystalline structure can be detected. This result reveals that the RGO sheets in hybrid are well separated and the RuO_2 is amorphous due to the low temperature of 150 ° C[2, 38]. To further confirm the composition of RuO_2 components in hybrid hydrogel, XPS measurement was performed. Fig 4(b) shows the comparative X-ray photoelectron spectroscopy (XPS) results of the as-prepared hybrid hydrogels. For the as-prepared samples, the C1s (284.5 eV) peak is clearly observed, this peak corresponds to the graphitic carbon atoms in graphene[39]. In the spectra of the hybrid hydrogels, Ru XPS signals such as 3p, 3d, 4s, and 4p appear in addition to the C1s and O1s signals corresponding to O-C bonds in graphene and O-Ru bonds in RuO_2. The oxidation state of ruthenium can be determined from narrow scans of the Ru 3d doublet (275-290 eV). Spectrum displays the characteristic shape of the Ru3d doublet, which exhibits two relatively narrow peaks corresponding to the 5/2 and 3/2 spin orbit components. Moreover, the Ru 3d5/2 peak appears at 281.0 eV corresponds to the binding energy of Ru^{4+} and further suggests the presence of RuO_2 in the composites[3] (see Fig S4).

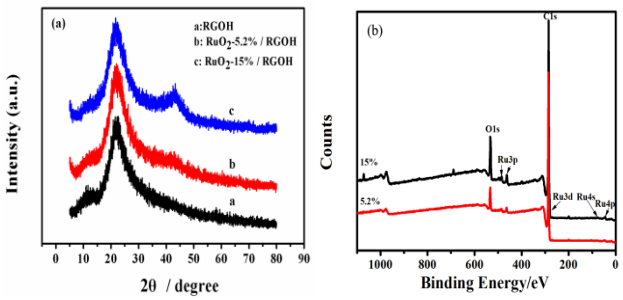

Fig. 4 (a) XRD of the products, (b) XPS of the RuO_2-15% / RGOH.

Electrochemical characterization

The electrochemical characteristics of these materials were studied through cyclic voltammetry (CV) using 1 M H_2SO_4 electrolyte, at potential window from 0-0.9 V. The result was presented in Fig 5. It can be clearly observed that the CV curves of all the three samples (Fig 5a) show a nearly rectangular voltammetric behavior and exhibit very broad redox peaks in the investigated potential region, which is indicative of a typical pseudocapacitive behavior of RuO_2. The specific capacitance is proportional to the maximal integral area of CV loop at the same scanning rate. From Fig 5a it can be seen the current densities increased with the content of RuO_2 in the hybrid hydrogels. That is to say, the specific capacitance of the hybrid hydrogels electrodes is obviously larger than that of the pure RGOH electrode at the same scan rate. The larger current density for hybrid hydrogels is due to the combination of the pseudocapacitance of RuO_2 with partially double-layer capacitance of graphene hydrogels. Here, the electronic-protonic "double insertion" mechanism of ruthenium oxide is expressed by the following redox reaction [40, 41],

$$RuO_x(OH)_y + \delta H^+ + \delta e^- \leftrightarrow RuO_{x-\delta}(OH)_{y+\delta} \quad (0 \le \delta \le 2) \ ,$$

where Ru oxidation states can change from (II) up to (IV). The CV curves of RuO_2/RGOH at different sweep rates are shown in Fig 5(b). As shown in Fig 5(b), CV profiles still retain a relatively

rectangular shape, even at a scan rate of 50 mV·s^{-1}, indicating an excellent capacitance behavior and the desirable fast charge/discharge property at the electrode interface.

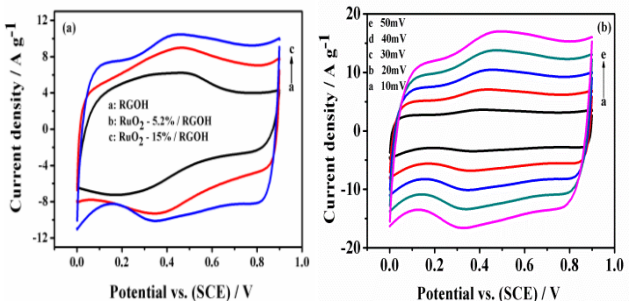

Fig. 5 CV curves of (a) RuO_2 / RGOH with different RuO_2 content, (b) The RuO_2 -15% / RGOH at different scan rates.

Fig 6(a) shows galvanostatic discharge curves of the pure RGOH and hybrid hydrogels in the potential range from 0 to 0.9 V (vs. SCE) at the current density of 1 A g^{-1}. The specific capacitance is calculated by the following equation $C = i \cdot t / \Delta V$, where i (A g^{-1}) is current density, t (s) is the discharge time, ΔV (V) is the applied potential window. According to the equation, the capacitances are 166, 246 and 345 F g^{-1} for pure RGO hydrogel, RuO_2-5.2% and RuO_2-15% electrodes, respectively. The overall capacitance of RuO_2/RGOH (C_{sp}) is composed of specific capacitance from RuO_2 (C_{RuO_2}) and RGO hydrogel (C_{RGOH}), which can be expressed as: $C_{sp} = C_{RuO_2} \times m + C_{RGOH} \times n$ [1], where m and n are the weight percentages of RuO_2 and RGO hydrogel in RuO_2/RGOH, respectively. According to the measured values of C_{sp} and C_{RGOH}, the values of C_{RuO_2} for RuO_2-5.2% and RuO_2-15% hybrid hydrogel electrodes were calculated to be 1365 and 1360F g^{-1}, respectively. Under the potential window selected in our experiment, theoretical specific capacitance of $RuO_2 \cdot xH_2O$ (for x=1) is 1419 F g^{-1}. Therefore, the utilization of RuO_2 is 95% at the current density of 1 A g^{-1}. The high utilization of RuO_2 is probably attributed to the synergistic effect between RuO_2 and RGOH. First, 3D interconnected porous graphene increase the liquid-solid interfacial area and facilitate H^+ transport within, which release double-layer capacitance of graphene. Second, the intimate combination of RuO_2 nanoparticles with electronically conducting graphene sheets provides electron superhighways, which allow for rapid and efficient charge transport. Finally, the well-dispersed fine RuO_2 nanoparticles on RGOH surfaces may be completely accessible to the electrolyte, which leads to the sufficient generation of RuO_2 pseudocapacitance.

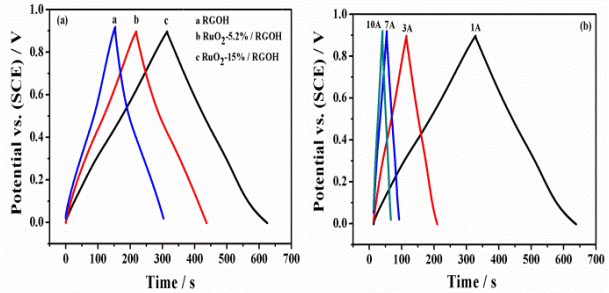

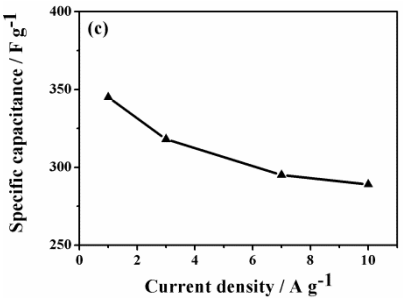

Fig. 6 The charge and discharge curves of (a) RuO_2 / RGOH at 1 A g^{-1}, (b) The RuO_2-15%/ RGOH at different specific currents, (c) Specific capacitance of the RuO_2-15%/ RGOH at various specific current.

Rate capability is an important power factor in the applications of supercapacitors, Fig 6(b) shows galvanostatic discharge curves of the RuO_2 /RGOH at various current densities. The specific capacitance of RuO_2 /RGOH is still up to 289 F g^{-1} at 10 A g^{-1}, with 83.7% retention relative to 1 A g^{-1}. This implies that the RuO_2/RGOH has a good rate capability at a large specific current. The superior rate capability in the RuO_2/RGOH electrode can be attributed to the three-dimensional porous network structure. In high charging-discharging rates, the electrodes can achieve higher charge mobility than non-porous counterpart. Moreover, the use of conductive graphene hydrogel as a substrate for growth of RuO_2 can impart the electrodes to excellent conductivity. The low resistances in the electrodes allow rapid and effective electrons transport, which may also contribute to high rate performances.

The electrochemical impedance spectroscopy (EIS) analysis has been recognized as one of the principal methods for examining the fundamental behavior of electrode material for supercapacitors[42]. Typical complex plane plots for RuO_2/RGOH and RGOH are presented in Fig 7(a), the frequency ranged from 0.1 Hz to 10 kHz at open-circuit potential of 0.4 V. At high frequency, the intersection on X-axis is a combinational resistance of ionic resistance of electrolyte, intrinsic resistance of substrate, and contact resistance at the active material/current collector interface. It is found that the RuO_2/RGOH has a similar series resistance to RGOH. The semicircle in the high-frequency range corresponds to the charge-transfer resistance, which is caused by the redox reactions of RuO_2 particles and residual oxygen-containing functional groups from graphene hydrogel. The sloped portion of the Nyquist plot at middle frequency is attributed to the Warburg resistance, which results from the frequency dependence of ion diffusion and transport in the electrolyte. At lower frequency, the imaginary part of impedance sharply increases, indicating the capacitive behavior of electrodes. The RuO_2/RGOH and RGOH all exhibit almost a vertical line at the low frequency region, suggesting the ideal capacitive behavior and have faster ion transport speed[42]. These attributed to the interconnected porous network, which can readily enable electrolyte ion diffusion and electron transport across the interface between RuO_2 and the graphene framework, thereby resulting in superior electrochemical activity and stability.

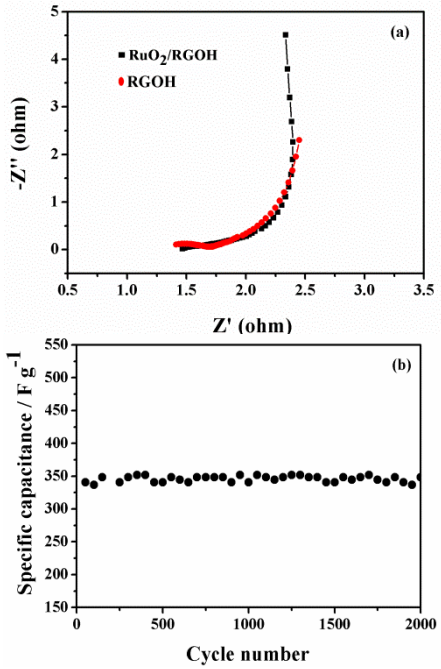

Fig. 7 (a) Nyquist plots of pure RGOH and RuO_2-15%/RGOH, (b)The cycle life of RuO_2-15% / RGOH.

Long cycling life is an important requirement for supercapacitors in practical applications. The cycling life test of the RuO_2/RGOH was examined by charge/discharge cycling at a current density of 1 A g^{-1}. As shown in Fig 7(b), the RuO_2/RGOH can maintain a specific capacitance of 346 F g^{-1} after 2000 cycles without decaying. This result indicates excellent electrochemical stability of such electrode material over the entire number of cycles. Usually, the capacitance loss of electrodes is mainly caused by phase transformation and structural degradation. In RuO_2/RGOH electrode, RuO_2 particles can be protected by the adjacent graphene sheets, which offer high mechanical durability and surface areas to inhibit agglomeration of RuO_2 particles. Moreover, the 3D network structure of the hybrid hydrogels can also improve the cycle life by providing stable conductive networks with high mechanical rigidity, which may afford elastomeric space to accommodate volume changes. The long-term stability implies that the RuO_2/RGOH material is a promising electrode material for supercapacitors.

Conclusions

The RuO_2/reduced graphene oxide hydrogel materials have been successfully prepared for supercapacitors through one-step hydrothermal self-assembly method by using $RuCl_3 \cdot xH_2O$ and graphene oxide as starting materials. In the composites, flexible graphene sheets partially overlap forming a porous network framework, well dispersed RuO_2 nanoparticles with 2 to 3 nm in size are homogeneously dispersed on the surface of the reduced graphene oxide sheets with the help of oxygen-containing functional groups. As compared with pure reduced graphene oxide hydrogel, the RuO_2/reduced graphene oxide hydrogel with 15wt% RuO_2 exhibits higher specific capacitance (345 F g^{-1}), remarkable rate capability and excellent cycle stability (without decaying after 2000 cycles). In addition, as compared with theoretical specific capacitance of RuO_2, the utilization of RuO_2 in the composite is as high as 95% at the current density of 1 A g^{-1}. Considering the advantages of graphene as EDLCs, RuO_2 as pseudocapacitors, complement each other's advantages between graphene and RuO_2, we believe that the novel particle/sheet structured RuO_2/reduced graphene oxide hydrogel can be applied in high performance energy storage systems.

Experimental

GO was synthesized through modified Hummers method[43]. The RuO_2/RGOH samples with different RuO_2 content were here prepared. The typical procedure (preparing the RuO_2/RGOH with 15% RuO_2) as follows: GO (80 mg) was exfoliated in distilled water (50 mL) with 1h ultrasonic treatment to form a light-brown solution. 3.5mL of $RuCl_3$ solution (20mg mL^{-1}) was dropped into GO solution with vigorous stirring. Under continuous stirring condions, the solution of 0.01 M NaOH was added drop-wise to neutralize the dispersion (up to pH 7). Then, the mixture was sealed in a Teflon-lined autoclave and maintained at 180 ℃ for 12 h. The autoclave was naturally cooled in room temperature, and then, a black cylinder was obtained. Finally, the black cylinder monolith was taken out, washed with a large amount of distilled water, and freeze-dried into a hydrogel. For comparison, other hybrid hydrogels with different RuO_2 loadings prepared by a similar procedure with adding different $RuCl_3$. Pure graphene hydrogel was prepared by the same procedure in the absence of $RuCl_3$.

The morphology of the products was characterized by field-emission scanning electron microscope (FESEM, JSM-6701F, Japan) and transmission electron microscope (TEM, JEOL, JEM-2010, Japan). The structure of the samples was characterized by X-ray diffraction (XRD, D/Max-2400) with Cu Kα radiation operating at 40 KV. The components and chemical state analysis was examined by X-ray photoelectron spectroscopy (XPS, PHI-5702, U. S. A.). The loading of RuO_2 on the RGOH was determined by using thermogravimetric (TG, TG/DTA-6300) analysis.

The electrochemical capacitive performances of hybrid hydrogel were performed on a typical three-electrode experimental cell, in which platinum foil and saturated calomelel ectrodes (SCE) were used as counter electrode and reference electrodes, respectively. All of the above electrochemical measurements were carried out by using a CHI660B electrochemical working station. All electrochemical measurements were carried out in 1 M H_2SO_4 aqueous solution as electrolyte.

Acknowledgements

The authors gratefully acknowledge the financial support offered by the National Natural Science Foundation of China (20963009 and 21163017), Specialized Research Fund for the Doctoral Program of Higher Education (No. 20126203110001).

Notes and references

Key Laboratory of Eco-Environment-Related Polymer Materials of Ministry of Education, Key Laboratory of Polymer Materials of Gansu Province, College of Chemistry and Chemical Engineering, Northwest

Normal University, Lanzhou, Gansu 730070, PR China, Tel.: +86 931 7973255; fax: +86 931 8859764 Email address: zhongai@nwnu.edu.cn

1 Y. D. Liu, F. Zhou, V. Ozolins, *J. Phys. Chem. C, 2012,* **116**, 1450.
2 Z. S. Wu , D. W. Wang, W. C. Ren, J. P. Zhao, G. M. Zhou, F. Li, H. M. Cheng, *Adv. Funct. Mater.*, 2010, **20**, 3595.
3 Y. T. Kim, K. Tadai, T. Mitani, *J. Mater. Chem.* 15 (2005) 4914-4921.
4 W. Sugimoto, H. Iwata, Y. Yasunaga, Y. Murakami, Y. Takasu, *Angew. Chem. Int. Ed.*, 2003, **42**, 4092.
5 M. Min, K. Machida, J. H. Jang, K. Naoiz, *J. Electrochem. Soc.*, 2006, **153**, A334.
6 Y. F. Su , F. Wu , L. Y. Bao , Z. H. Yang, *New Carbon Mater.*, 2007, **22**, 57.
7 H. T. Fang, M. L, D. W. Wang, X. H. Ren, X. Sun, *Nano Energy*, 2013, **2**, 1232.
8 S. C. Yan, H. T. Wang, P. Qu, Y. Zhang, Z. D. Xiao, *Synth. Met.*,*2009*, **159**, 158.
9 Y. C. Su, C. A. Chen, Y. M. Chen, Y. S. Huang, K.Y. Lee, K. K. Tiong, *J. Alloys Compd.*, 2011, **509**, 2011.
10 T. F. Hsieh, C. C. Chuang, W. J. Chen, J. H. Huang, W. T. Chen, C. M. Shu, *Carbon*, 2012, **50**, 740.
11 M. Kang, Y. Lee, H. Jung, J. H. Shim, N. S. Lee, J. M. Baik, S. C. Lee, C. Lee, Y. Lee, M. H. Kim, *Anal. Chem.*, 2012, **84**, 9485.
12 V. Barranco, F. Pico, J. Ibañez, M. A. Lillo-Rodenas, A. Linares-Solano, M. Kimura, A. Oya, R. M. Rojia, J. M. Amarilla, J. M. Rojo, *Electrochim. Acta*, 2009, **54**, 7452.
13 F. Pico, J. Ibañez, M. A. Lillo-Rodenas, A. Linares-Solano, R.M. Rojas a, J.M. Amarilla a, J.M. Rojo, *J. Power Sources*, 2008, **176**, 417.
14 C. M. Chuang, C. W. Huang, H. Teng, J. M. Ting, *Compos. Sci. Technol.*, 2012, **72**, 1524.
15 N. Lin, J. H. Tian, Z. Q. Shan, K. Chen, W. M. Liao, *Electrochim. Acta*, 2013, **99**, 219.
16 H. G. Jung, Y. S. Jeong, J. B. Park, Y. K. Sun, B. Scrosati, Y. J. Lee, *ACS Nano* 4 (2013) 3532-3539.
17 L. J. Deng, J. F. Wang, G. Zhu, L. P. Kang, Z. P. Hao, Z. B. Lei, Z. P. Yang, Z. H. Liu, 2014, **248**, 407.
18 L. X. Zhou, J. M. Xue, Y. G. Wang, G. X. Cao, *Carbon*, 2013, **6**, 117.
19 J. Hofrichter, B. N. Szafranek, M. Otto, T. J. Echtermeyer,M. Baus, A. Majerus, V. Geringer, M. Ramsteiner, H. Kurz, *Nano Lett.*, 2010, **10**, 36.
20 D. C. Wei, Y. Q. Liu, Y. Wang, H. L. Zhang, L. P. Huang, G. Yu, *Nano Lett.*, 2009, **5**, 1752.
21 Y. H. Wu, C. X. Guo, N. Li, L. L. Ji, Y. W. Li, Y. F. Tu , X. M. Yang, *Electrochim. Acta,* 2014, **146**, 386.
22 B. Wang, S. M. Li, J. H. Liu, M. Yu, B. Li, X.Y. Wu, *Electrochim. Acta*, 2014, **146**, 679.
23 X. Chen, C. L. Long, C. P. Lin, T. Wei, J. Yan, L. L. Jiang, Z. J. Fan, *Electrochim. Acta, 2014,* **137**, 352.
24 S. Guo, G. K. Zhang, Y. D.Guo, J. C. Yu, *Carbon*, 2013, **60**, 437.
25 Y. Y. Yang, Z. A. Hu, Z. Y. Zhang, F. H. Zhang, Y. J. Zhang, P. J. Liang, H. Y. Zhang, H. Y. Wu, *Mater. Chem. Phys., 2012*, **133**, 363.
26 Y. L. Chen, Z. A. Hu, Y. Q. Chang, H. W. Wang, Z. Y. Zhang, Y. Y. Yang, H. Y. Wu, *J. Phys. Chem. C*, 2011, **115**, 2563.
27 H. W. Wang, Z. A. Hu, Y. Q. Chang, Y. L. Chen, Z. Y. Zhang, Y. Y. Yang, H. Y. Wu, *Mater. Chem. Phys.*, 2011, **30**, 672.
28 H. W. Wang, H. Yi, X. Chen, X. F. Wang, *J. Mater. Chem. A*, 2014, **2**, 1165.
29 Z. S. Wu, Y. Sun, Y. Z. Tan, S. Yang, X. L. Feng, K. Müllen, *J. Am. Chem. Soc.*, 2012, **134**, 19532.
30 V. H. Luan, J. S. Chung, E. J. Kim, S. H. Hur, *Chem. Eng. J.*,*2014*, **246**, 64.
31 H. Zhou, W. Yao, G. Li, J. Wang, Y. Lu, *carbon*, 2013, **59**, 495.
32 L. J. Li, S. Y. Liu, A. Manthiram, *Nano Energy,* 2014, http://dx.doi.org/10.1016/j.nanoen.2014.10.036
33 C. C. Ji, M. W. Xu, S. J. Bao, Z. J. Lu, C. J. Cai, H. Chai, R. Y. Wang, F. Yang , H. Wei, *New J. Chem.*, 2014, **37,** 4199.
34 W. Wang, S. R. Guo, I. Lee, K. Ahmed, J. B. Zhong, Z. Favors, F. Zaera, M. Ozkan, C. S. Ozkan, *Sci. Rep.*, 2014, **4**, 4452.
35 H. C. Gao, Y. M. Sun, J. J. Zhou, R. Xu, H. W. Duan, *ACS Appl. Mater. Interfaces, 2013,* **5**, 425.
36 H. C. Gao, F. Xiao, C. B. Ching, H. W. Duan, *ACS Appl. Mater. Interfaces, 2012,* **4**, 2801.
37 Y. X. Xu, K. X. Sheng, C. Li, G. Q. Shi, *ACS Nano, 2010,* **4**, 4324.
38 C. C. Hu, W. C. Chen , K. H. Chang, *J. Electrochem. Soc., 2014,* **151**, A281.
39 H. C. Schniepp, J. L. Li, M. J. McAllister, H. Sai , M. Herrera-Alonso, D. H. Adamson, R. K. Prud'homme, R. Car, D. A. Saville, I. A. Aksay, *J. Phys. Chem. B,* 2006 , **110** , 8535.
40 S. Trasatti, Physical electrochemistry of ceramic oxides, *Electrochim. Acta, 1991,* **36**, 225.
41 Y. D. Liu, F. Zhou, V. Ozolins, *J. Phys. Chem. C, 2012,* **116**, 1450.
42 S. Park, J. An, R. D. Piner, I. Jung, D. Yang, A.Velamakanni, S. T. Nguyen, R. S. Ruoff, *Chem. Mater., 2008,* **20**, 6592.
43 W. S. Hummers, R. E. Offeman, *J. Am. Chem. Soc.*, 1958, **80**, 1339.